Mon. Not. R. Astron. Soc. **000**, 000–000 (0000) Printed 9 October 2008 (MN LATEX style file v2.2)

Near-infrared polarimetry of the Red Rectangle

T.M. Gledhill[1⋆], A.N. Witt[2], U.P. Vijh[2], C.J. Davis[3]
[1] *Science and Technology Research Institute, University of Hertfordshire, College Lane, Hatfield AL10 9AB, England*
[2] *Ritter Astrophysical Research Center, University of Toledo, Toledo, OH 43606, USA*
[3] *Joint Astronomy Center, 660 N. A'Ohoku Place, Hilo, HI 96720, USA*

9 October 2008

ABSTRACT
Imaging polarimetry through J and H broad-band filters and a 3.4 μm narrow-band filter is used to highlight regions of scattered light in the Red Rectangle. We find that the scattered light identifies the circumbinary dust component of the molecular disc seen in CO emission. This region also appears to be the origin of the recently discovered Blue Luminescence. We find that the degrees of polarization are consistent with the amorphous carbon dust model invoked by Men'shchikov et al. (2002). Spectropolarimetry from 1.4 to 2.5 μm confirms that the degree of polarization in the central arcsecond region is very low. This suggests that the central bicone seen in the near-infrared is due predominantly to emission from hot dust and/or from stochastically heated nanoparticles, rather than due to scattering by large grains.

Key words: techniques: polarimetric – circumstellar matter – scattering – stars: AGB and post-AGB – stars: individual: HD 44179

1 INTRODUCTION

The Red Rectangle (RR) is a well known proto-planetary nebula (PPN), originally identified by Cohen et al. (1975), although its evolutionary status was uncertain at that time. The nebula has resulted from rapid mass loss from a centrally embedded binary (van Winckel, Waelkens & Waters 1995) in which the luminous component is the post-AGB star HD 44179. It has been suggested that the companion to HD 44179 is a white dwarf (Men'shchikov et al. 2002), although recent spectroscopic monitoring by Witt et al. (2008) shows that it is most likely a main-sequence star.

Dust and molecules in the nebula produce a rich spectrum of emission features including the broad Extended Red Emission (ERE) continuum (Schmidt et al. 1980) and the more recently discovered Blue Luminescence (BL) (Vijh et al. 2004). The RR is the brightest source of unidentified infrared (UIR) bands (Cohen et al. 1975; Russell, Soifer & Willner 1978), now generally attributed to polycyclic aromatic hydrocarbons (PAHs) and their ions (Allamandola, Tielens & Barker 1985). Optical imaging observations using the WFCAM2 aboard *HST* have revealed intricately detailed structure in the nebula, which has an extent of at least 2 armin on the sky (Cohen et al. 2004). Maps of CO J=2-1 and J=1-0 transitions show that the molecular envelope deviates significantly from spherical symmetry within a radius of 2.5 arcsec, appearing as a disc oriented at position angle (PA) 101°, perpendicular to the axis of the bipolar nebula (Bujarrabal et al. 2003). Model fits to the CO data suggest that the inner parts of this disc may be in stable Keplerian rotation (Bujarrabal et al. 2005).

A model for the circumbinary material in the RR has been proposed by Men'shchikov et al. (2002; hereafter M02), in which a common envelope ejection event has resulted in an optically thick dusty envelope surrounding the stars. Bipolar cavities in this spherical envelope allow light from the stars to escape to illuminate and excite dust and molecules in their walls, producing the striking bipolar nebula seen at optical and infrared wavelengths. The system is seen almost edge-on so that the central stars remain totally obscured to Earth-based observers. While the model is simplistic in the assumption of a spherically symmetric dust distribution, and does not include the BL, ERE or PAH emission, it otherwise successfully accounts for the UV to radio continuum SED. The model also simulates the appearance of near-infrared speckle interferometry images of the central sub-arcsecond region (Men'shchikov et al. 1998), which show bipolar lobes separated by a dark obscuring lane.

In this paper we further explore the distribution and nature of the dust in the RR by using near-infrared polarimetry to highlight regions of scattered light relative to non-scattered emission. We consider whether the degrees of polarization detected are consistent with the dust model used to fit the SED.

⋆ E-mail: t.gledhill@herts.ac.uk

2 OBSERVATIONS AND DATA REDUCTION

Polarimetric observations were made with the UIST imager/spectrometer (Ramsay Howatt et al. 2004) at the 3.8-m UK Infrared Telescope (UKIRT) in February, March and October 2006, and are summarized in Table 1. Weather conditions were poor with variable levels of cloud cover, so that flux calibration has not been possible. Estimates of the image quality, in terms of the FWHM of the PSF are given in Table 1. The spectropolarimetry was undertaken as a bad weather backup in thick and variable cloud.

2.1 Instrument setup

Imaging polarimetry was obtained through the J and H broad-band filters from the Mauna Kea filter set, and the 3.4nbL narrow-band filter. The image scale was 0.12 arcsec per pixel. To measure polarization, a rotating half-wave retarder (IRPOL2) located above the telescope dichroic was used in conjunction with a fixed Wollaston prism and focal plane mask, mounted within UIST. A single achromat retarder was used between 0.9 and 2.5 μm and a zero-order retarder tuned to 3.6 μm was used for the nbL imaging. This standard configuration for dual-beam polarimetry is described further on the UKIRT web pages[1].

One modification to the standard set up was the inclusion of a piece of wire fixed across the focal plane mask, to act as a rudimentary coronagraph. This allowed the very bright central point source of the RR to be obscured, thus enabling longer exposure times on the fainter surrounding nebulosity without saturating the detector. In addition, unmasked images of the central region were made with the J and 3.4nbL filters. The mask used for the H-band observations consisted of a N-S oriented 0.5 arcsec diameter wire. A new mask was installed prior to the 2006 October run, with a 0.7 arcsec diameter E-W oriented wire, and this was used for the J-band coronagraphic observations.

Spectropolarimetry used the HK grism, covering a wavelength range of $1.395 - 2.506$ μm with a spectral resolution of 900, and a 2 pixel-wide slit oriented 120° East of North. These observations used the same half-wave retarder and Wollaston prism setup as for imaging, with the exception that eight orientations of the retarder are used (rather than four as for imaging) in order to eliminate any ripple structure in the polarization spectrum (Aitken & Hough 2001).

2.2 Data reduction and calibration

Data reduction for imaging consisted of debiasing, flatfielding using dome flatfields, and alignment and processing of images using the POLPACK software package to produce images of the Stokes intensities I, Q and U. In the case of the J-band imaging, the three sets of data with exposure times of 0.9 sec, 5 sec and 10 sec were combined to produce a single data set providing information on the central peak of the RR (0.9 sec non-coronagraphic images) and on the outer nebulosity (5 and 10 sec coronagraphic images).

A polarized standard star, HD 38563 (Whittet et al. 1992), was observed to calibrate the polarization position angle on the sky. A correction of -24.7 degrees is applied to the measured UIST polarization position angles, which agrees well with the mean value of -24 degrees quoted on the UKIRT web pages.

Spectropolarimetry data was first processed through the ORACDR pipeline software to produce flatfielded and wavelength calibrated images. The spectra were then sky subtracted, optimally extracted and processed through POLPACK to form data cubes containing the I, Q and U spectral intensities. Atmospheric correction was achieved using observations of the F4V standard HIP 28854.

Table 1. Summary of the Red Rectangle observations, including the filter/grism used, the wavelength range (50% cut on/off point for the filters), date of observation, and exposure time/total integration time (seconds). An indication of the PSF size and shape is given (FWHM in arcsec along a N-S and E-W axis) using field stars unless otherwise indicated.

Filter	$\Delta\lambda$ (μm)	UT Date	Exp/Int	PSF ($''$)
J[MK]	1.17-1.33	20060308	0.9/648	0.79×0.78
		20061009[c]	5/1440	0.72×0.72
		10061009[c]	10/720	0.63×0.60
H[MK]	1.49-1.78	20060212[c]	10/480	-[1]
3.4nbL	3.379-3.451	20061009	3/1080	0.80×0.65[2]
HK spec	1.395-2.506	20061010	7/560	-

[c] : coronagraphic mask used
[1] No centroid available; [2]: Red Rectangle peak used.

3 RESULTS

3.1 Imaging polarimetry

The imaging polarimetric results are shown in Fig. 1. The H-band observations used a wire coronagraph, to block out the central bright peak of the RR. The affected pixels have been set to zero, resulting in the white stripe seen in the images. Despite the mask, there are still some saturated pixels around the centres of the H-band images. The J-band observations included short-exposures without the coronagraph, in addition to the longer coronagraphic exposures, and these two sets have been normalized and median stacked to form the J-band images. The noisy horizontal stripe, visible in the outer regions of the J-band polarized flux and per cent polarization images, results from the combination of these long exposure coronographic and short exposure non-coronographic data sets.[2] The nbL images are taken without the coronagraph.

The intensity distribution in the J- and H-band filters appears very point source-like, with no hint of the dramatic X-shaped structure seen at shorter wavelengths (particularly the ERE-emitting wavelengths peaking around 670 nm). In fact, in the J-band, where we have observed the unsaturated central peak, the FWHM of the intensity distribution is 0.9 arcsec, which is only marginally broader than that measured from a standard star (Table 1). High spatial resolution speckle interferometry observations in the H-band (Men'shchikov et al. 1998; Tuthill et al. 2002) show two

[1] http://www.jach.hawaii.edu/UKIRT/

[2] As mentioned in Section 2.1, the coronograph wire orientation was East-West for the J-band and North-South for the H-band.

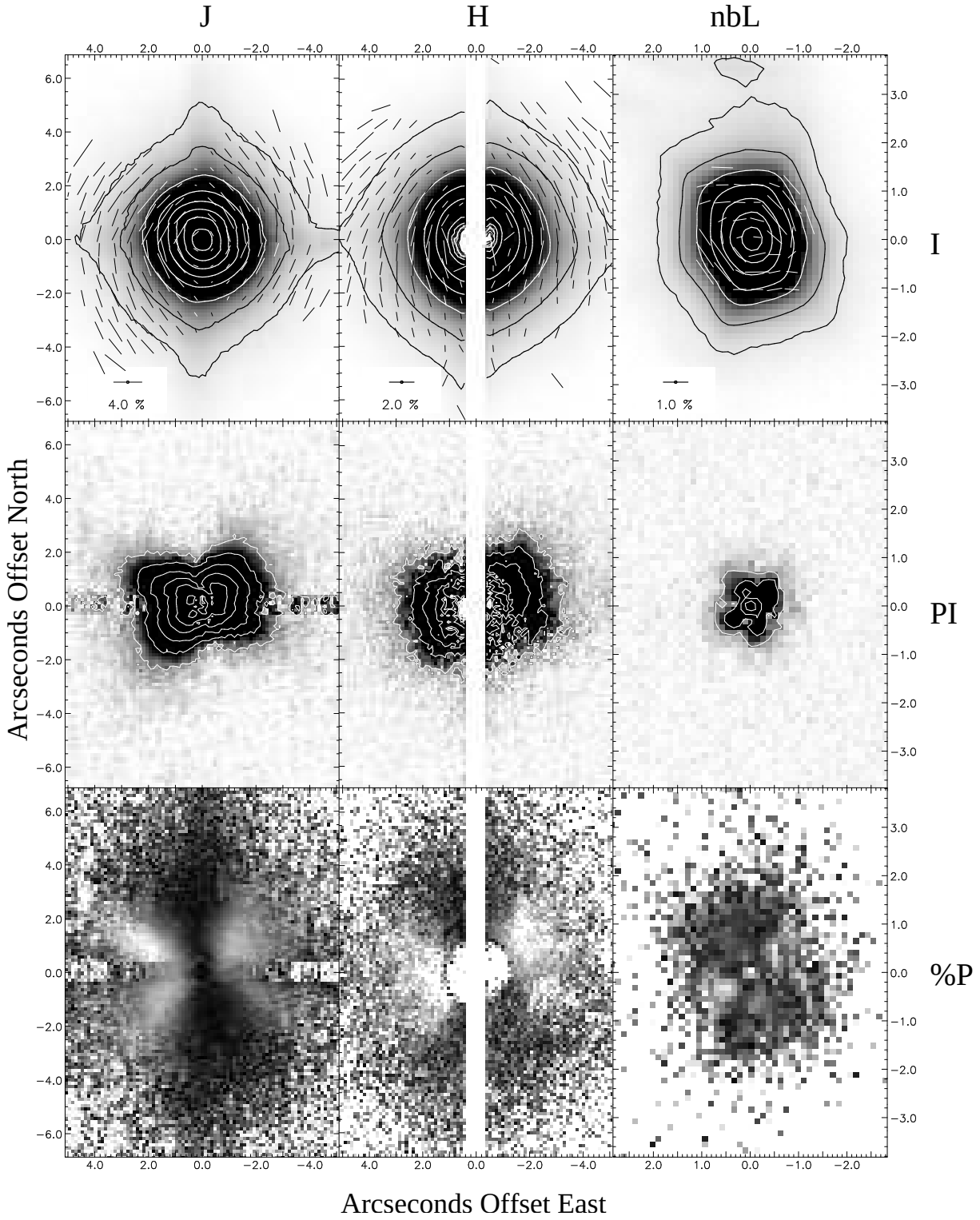

Figure 1. *Upper:* Polarization vector plots through the three filters, superimposed on greyscale intensity images. North is up and east left. The H-band observations used a wire strip to mask the central object and this appears as the light-coloured strip in the image. Contours are spaced at 1 magnitude intervals, with the first contour at $20\sigma_{\rm sky}$.*Middle:* Polarised intensity images and contours. Contours are spaced at 1 magnitude intervals with the first contour at $10\sigma_{\rm sky}$. *Lower:* Percent polarization images. Black corresponds to P=0 per cent and white to P=5 per cent (J) and P=2 per cent (H and nbL) respectively. Note that the nbL data are plotted on an expanded spatial scale.

bright lobes separated by a narrow dark lane at the centre of the RR, on a scale of less than an arcsec, which is unresolved in our data. We have performed a rough deconvolution of the J-band peak[3], using the polarized standard star as a PSF reference, and find it to be elongated along a PA between 10 and 20 degrees. This is consistent with the orientation of the bipolar lobes at PA 12 degrees seen in the diffraction-limited H- and K-band speckle images of Men'shchikov et al. (1998). Any nebular emission in our J- and H-band images is, therefore, dominated by the PSF of these bright, unresolved bipolar lobes, whose PSF wings extend to a radius of 5 arcsec. This is further confirmed by inspection of the outer regions of the polarized standard star images, which show the same "diamond-shaped" outer contour due to the telescope's diffraction spikes.

In the 3.4 μm nbL filter, the object assumes a more rectangular appearance, although the emission is still strongly peaked towards the centre. Clearly, the PSF does not dominate in this waveband, and we see emission from extended nebulosity, with the major axis oriented at PA 15 degrees. The X-shaped bicone edges are just visible in our image.[4] The nebula has a similar appearance in the L′- (3.87 μm) speckle images of Mékarnia et al. (1998), being centrally peaked and elongated along PA 13°. In fact, the RR shows a consistent morphology throughout the near- and mid-infrared, both in continuum and in the UIR bands (**Miyata et al. 2004;** Mékarnia et al. 1998; Hora et al. 1996). The well known 3.3 μm emission band, commonly attributed to C-H bond stretching, is seen strongly in the RR. However, inspection of the band profile in Song et al. (2003) shows that the 3.3 μm emission lies outside our nbL filter bandpass, so that we are imaging the near-infrared continuum in this filter.

In all three filters the polarization vectors show a centrosymmetric pattern typical of light that originates from a central source and is then scattered in a circumstellar dust shell. Scattered light is detected out to a radius of approximately 5 arcsec in the J- and H-bands. The degrees of polarization are in the range 2 to 4 per cent in the J-band dropping to 1 to 2 per cent at longer wavelengths. This is **consistent with previous near-infrared measurements (Jones & Dyck 1978) but is** unusually low for reflection nebulosity associated with post-AGB stars, where linear polarizations of 20 per cent or more are commonly observed in the near-infrared (e.g. Gledhill et al. 2001; Gledhill 2005). However, in the J- and H-bands the overlying PSF (resulting from the central bright peak) dominates the scattered intensity from the nebula, and if it is unpolarized then it will dilute the intrinsic polarization of the scattered light. In the nbL data, we attribute the low polarization to dilution by an unpolarized infrared continuum, which increases in strength with wavelength beyond 1 μm and which dominates the scattered light component at 3.4 μm. We discuss the nebula polarization and the role of particle emission further in Section 4.2.

[3] A Lucy-Richardson deconvolution was used, as implemented by the IDL procedure LUCY.PRO, which is part of the NICMOS library developed at the University of Arizona.

[4] The faint patch to the N of the object is an artifact associated with the telescope optics.

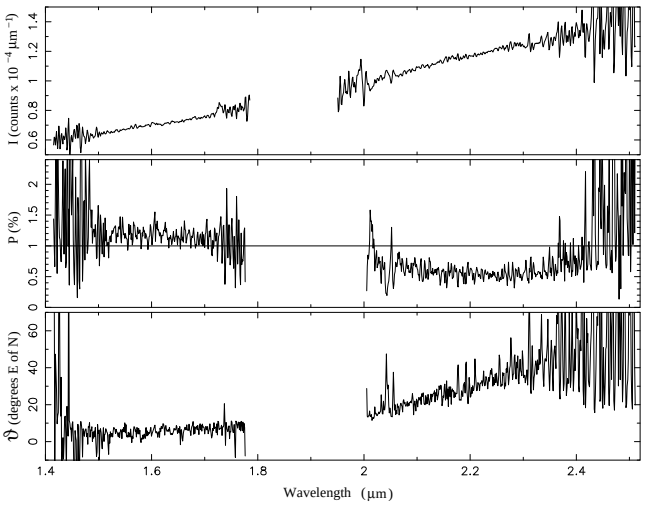

Figure 2. Longslit spectropolarimetry of the RR. The region of poor atmospheric transmission, between 1.8 and 2 μm has been removed.

3.2 H-K Spectropolarimetry

Spectropolarimetry of the RR is shown in Fig. 2 and has been summed along the slit, so that it is dominated by the central bright peak. The intensity spectrum shows a featureless continuum rising into the red, in agreement with previous 1.4-2.3 μm spectroscopy (Thronson 1982). Residual features in the spectrum are likely to result from imperfect correction for atmospheric lines due to the poor observing conditions at the time. The continuum continues to rise beyond our spectral range, where it is superimposed with the various UIR bands (Waters et al. 1998). The per cent polarization spectrum shows that the degree of polarization in the central peak decreases with increasing wavelength, from approximately 1.2 per cent at 1.6 μm to 0.5 per cent at 2.5 μm.[5]. This is again consistent with the argument that the rising infrared continuum is unpolarized and increasingly dominates at longer wavelengths over the scattered light component in the central (1 arcsecond) region of the RR. The PA of polarization lies between 5 and 10 degrees in the H-band region (roughly parallel to the bicone axis), rotating to larger angles at longer wavelengths.

4 DISCUSSION

The three principal findings of our observations are (i) the elongated distribution of the scattered light, (ii) the low degrees of nebular polarization in the infrared, and (iii) the non-detection of polarized emission from the central bicone. In the next section we compare the scattered light distribution to the distribution of molecular material in the RR and to imaging observations at optical wavelengths. In Section 4.2, we discuss the nebular polarization within the context of the dust grain model of M02, and the possible role of non-scattered nebular emission from

[5] Note that the spectropolarimetric measurements are integrated over a 2 pixel-wide (0.24 arcsec) slit

transiently heated small particles. In Section 4.3 we consider the nature of the emission from the central bicone.

4.1 The distribution of scattered light

The polarized intensity images (Fig. 1 middle) show that, in the J- and H-bands, polarized light emanates mainly from an elongated region, centred on the total intensity peak, with the long axis oriented at PA 100°. This orientation is perpendicular to the axis defined by the large-scale nebula seen in the light of ERE and to that defined by the sub-arcsecond-scale bipolar lobes (Cohen et al. 2004; Men'shchikov et al. 1998). The relative locations of the polarized emission and the ERE are shown in Fig. 3, with the polarized emission encompassing the equatorial region of the ERE bicone. Tracing this emission to 3 times the noise level in the J-band polarized flux image, its extent is 7.2 arcsec along a PA of 100 degrees and 4.8 arcsec in the perpendicular direction (5,100 and 3,400 au assuming the distance of 710 pc given by M02). There is evidence for fainter polarized emission surrounding this, which in the J-band has a "bow-tie" appearance, extending some way along the walls of the bicone. However, it is clear from Fig. 3 that we have not detected polarized light within the bicones or along their edges in the near-infrared.

We identify the polarized light with scattering within a dusty envelope, which is aligned with, but larger than, the rotating molecular structure discovered in CO observations by Bujarrabal et al. (2003, 2005). These authors fit their CO data with a disc model having outer radius 2.54 arcsec and constant thickness 1.41 arcsec (1,800 and 1000 au), oriented with the long axis along PA 101 degrees. These large-scale dust and gas structures then surround the sub-arcsecond-scale dark lane and bipolar lobes at the centre of the RR, which are modelled as a 100 au-radius optically thick shell with biconical cavities by M02. This shell surrounds and obscures the central binary.

The morphology of the RR is known to differ strikingly with wavelength. In the blue it appears as a spherically symmetric halo in *HST* images (F467M filter), with no hint of the X-shaped spikes, wine glass structures or ladders that are visible in the ERE band (540–750 nm). This blue halo is identified with scattered light and the surface brightness falls off as $r^{-2.7}$, consistent with an optically thin dust envelope with density profile close to r^{-2} (Cohen et al. 2004). The J- and H-band scattered light occupies roughly the same region as the blue halo and it is tempting to identify both blue and near-IR emission as scattering from the same dust particles. The blue light appears slightly more extended, visible to a radius of greater than 5 arcsec, and is spherically symmetric to a high degree, whereas the near-IR scattered light appears less extended and has a flattened distribution. However, it has to be borne in mind that we are comparing blue total intensity with near-IR polarized intensity. If the size distribution contains a significant number of sub-micron-sized grains then their scattering cross-sections will be larger in the blue than the infrared, resulting in a more spatially extended blue nebula. In addition, if the scattering asymmetry parameter, g, is significantly forward throwing, then the polarized intensity and total intensity images resulting from the same dust distribution can appear quite different. This is the case for the size distribution of amorphous carbon dust particles used by M02 to model the SED of the RR.

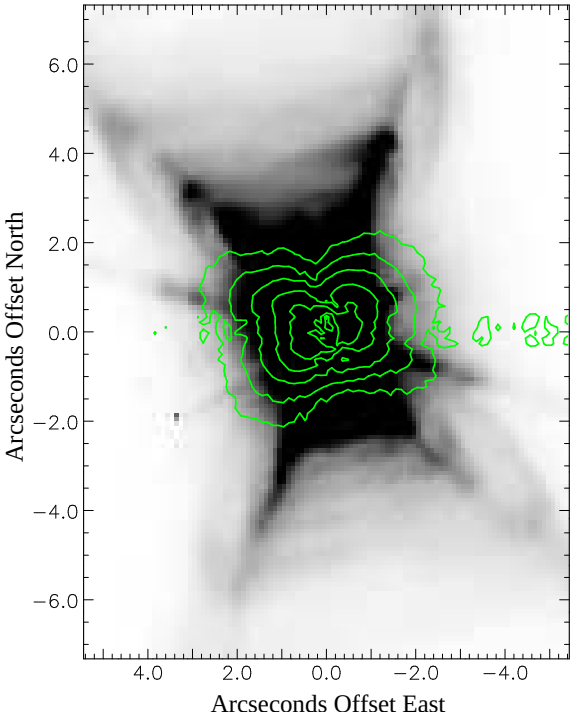

Figure 3. J-band polarized intensity contours superimposed on the F631N *HST* image of Cohen et al. (2004), showing the relative locations of the near-infrared polarized light and the ERE-emitting regions.

Narrow-band imaging close to the peak wavelength of the BL emission (393.4 nm) shows an extended (6 arcsec) region of emission with elongated central isophotes, oriented at PA 90° (Vijh et al. 2006). The orientation and extent is similar to that of the J-band scattered light (7.2 arcsec, PA 100°) and of the CO emission (5.7 arcsec, PA 101°). Vijh et al. (2006) suggest that the BL results from fluorescing neutral PAH molecules which can only exist in the equatorial regions of the RR, where they are shielded from high energy photons. Elsewhere, within the bicones for example, these PAHs are ionized and emit principally in the ERE bands. This supports our argument that the J- and H-band scattered light identifies the dust component of the extended circumbinary envelope seen in CO, and that this offers the protective environment required by the neutral PAHs responsible for the BL.

At longer wavelengths, in the nbL band, the polarized light is confined to the central region (1 arcsec radius). This can be understood if the dust particles responsible for scattering at J and H are less efficient scatterers at 3.4 μm (as is the case for the M02 size distribution), resulting in a lower scattering optical depth and a smaller reflection nebula. The nbL data also shows polarization in regions along the axis of the bicone (PA 11°), which appear unpolarized in the J-band data, perhaps indicating an additional component of polarization at longer wavelengths. This is supported by the HK spectropolarimetry data, in which the integrated polarization rotates in PA across the K-band (Fig. 2). The X-shaped spikes are just visible in the nbL intensity image,

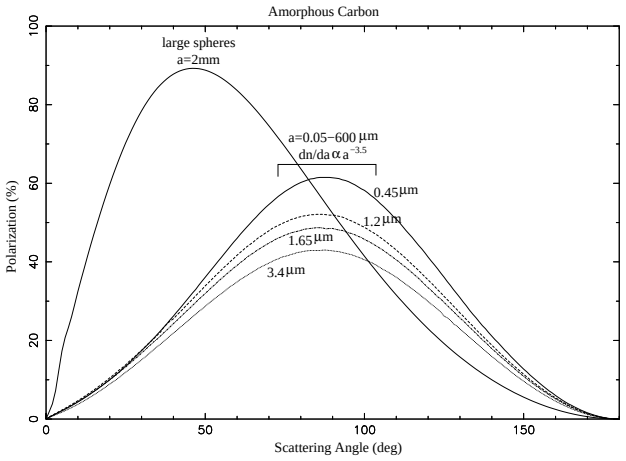

Figure 4. Polarization versus scattering angle plots for amorphous carbon grains, showing a single-size 2 mm sphere along with a size distribution of smaller grains at 4 wavelengths (0.45, 1.2, 1.65 and 3.4 μm).

but are unpolarized showing that they result from particle emission at this wavelength and not from scattering.

4.2 The nebula polarization and dust properties

Perkins et al. (1981) present optical imaging polarimetry of the RR using blue (400–500 nm) and red (610–750 nm) filters. Their data covers two 10 arcsec wide east-west strips located 10 arcsec north and south of the RR centre and they measure polarization of up to 20 per cent in the blue in the area of the bicones. They note that the X-shaped spikes are not visible in their direct blue images[6] but are seen in blue polarized intensity images. Perkins et al. conclude that the spikes result from a dust enhancement on the surface of the bicones combined with a forward-throwing dust scattering function (high scattered intensity at small scattering angle). This highlights the ability of imaging polarimetry to pick out polarized structures close to the plane of the sky, which are dominated in direct images by less polarized and brighter forward-scattered light from foreground sections of the line-of-sight.

M02 model the region outside the $r < 100$ au circumbinary torus as a spherical envelope with biconical cavities, containing amorphous carbon grains with radii between 0.005 and 600 μm, with an interstellar-type size distribution of $\mathrm{d}n/\mathrm{d}a \propto a^{-3.5}$. Assuming the refractive indices given by Preibisch et al. (1993) this dust model is forward-throwing at 450 nm, with an asymmetry parameter of $g = 0.67$, so could conceivably result in the presence of the spikes in blue polarized flux images, but their absence in direct images. The dust model is also highly polarizing, with a peak polarization of 62 per cent at a scattering angle of 88 degrees. Even taking into account dilution of this peak polarization due to scattering through a broad range of angles along a line of sight through a spherical nebula, the dust model could easily account for the observed 20 per cent polarization in the blue (Fig. 4). In the near-IR, at 1.2, 1.65 and 3.4 μm, the maximum polarizations from this dust are also high, peaking at 52, 49 and 43 per cent, respectively, so that the intrinsic polarization in the nebula must be significantly higher than our measured J, H and nbL polarizations of a few per cent. This supports the conclusion of the previous section that the scattered light from the nebula in the J- and H-bands is dominated by the wings of the PSF from the unresolved (in our observations) central bicone and that this PSF component is unpolarized.

There is also evidence for an oxygen-rich component in the RR. **Reese & Sitko (1996) identify features in their UV spectropolarimetry that may be attributable to OH.** Waters et al. (1998) detect features from crystalline silicates such as olivines and pyroxines in the equatorial region, roughly coincident with our region of near-infrared polarized flux. The question then arises whether this crystalline material would also be consistent with the observed polarization. A size distribution of silicates, such as that used for amorphous carbon in Fig. 4, would produce much lower polarization, since the peak polarization for a dielectric material oscillates between positive and negative values as a function of size parameter (e.g. Lucas & Roche 1998 Fig. 13). However, it is not clear that the silicate material in the RR should have the same size distribution as the carbon-rich dust, and the polarization would be much higher if only small (sub-micron) silicate grains are present. In addition, Waters et al. (1998) estimate that only 13 per cent of the dust in the extended nebula is in the form of crystalline silicates, so we expect that a combined carbon/silicate dust mixture would still be consistent with the observed polarization.

We must also consider the possibility that there is a contribution to the nebular intensity in the J- and H-bands from unpolarized dust emission and that this also reduces the observed polarization. The RR is well known as a strong source of particle emission in the blue (BL), optical (ERE) and in the UIR bands in the near- and mid-infrared. The infrared spectrum of the RR also shows a strong increase in non-photospheric continuum with wavelength, beginning at approximately 1 μm and extending to beyond the L-band. Similar infrared continuum emission has been observed in a variety of visual reflection nebulae, beginning at 1 μm and extending in some cases to 25 μm (Sellgren, Werner & Allamandola 1996 and references therein). The excess, often observed in combination with the 3.3 μm feature, cannot result from dust grains in thermal equilibrium with the illuminating star, and has been attributed instead to emission from tiny particles ($\sim$ 1 nm) that are transiently heated by absorption of single stellar photons. This emission can dominate over scattered light in the infrared, resulting in a reduction in the observed polarization. This has been observed specifically in NGC 7023, an optically thin reflection nebula associated with the star HD 200775, in which a peak polarization of 26 per cent is seen at J, which then decreases rapidly to values of 4-7 per cent at K (Sellgren, Werner & Dinerstein 1992). This wavelength behaviour of polarization is similar to that observed in the RR. Since the small-particle emission only becomes apparent beyond 1 μm, it is unlikely to contribute significantly to the reduction in J-band polar-

[6] They are also clearly absent in the much higher spatial resolution *HST* images of Cohen et al. 2004, where the RR appears roughly spherical in the blue.

ization, and instead in the case of our observations, this is heavily supressed due to the overlying PSF wings. However, we cannot rule out an extended component of small-particle emission at H. To investigate this further would require removal of the PSF, which is not possible with the data at present. The degree of polarization continues to drop beyond H and is typically only 1 per cent in the central 1 arcsec radius region in the nbL data. Since the PSF wings do not dominate here, as evidenced by the bipolar nebula shape, we can say with confidence that unpolarized dust emission contributes significantly in this band.

4.3 The central bicones and large grains

There is evidence for the presence of large grains at the centre of the RR. Jura, Turner & Balm (1997) find that the extended radio and millimetre emission is consistent with a bound disc containing particles with radii $\geqslant 0.02$ cm. In the model of M02, the bright central bicone results from scattering and emission from dust in the walls of cavities excavated in the dense circumbinary (100 au-radius) envelope. In order to account for the similar appearance of the bicone, from the blue through to the L-band, they find that very large (2 mm-radius) dust grains with grey extinction properties are necessary. **M02 also suggest that the biconical appearance of the nebula in the mid-infrared is due to scattering by very large grains. However, Miyata et al. (2004) show that the N-band emission is in fact dominated by UIR emission and not scattered light.**

As mentioned above, the scattered light in our J- and H-band observations is dominated by the PSF from this bright central bicone, and this PSF appears to be unpolarized. Fig. 1 shows that the degree of polarization drops to 1 per cent and below in the central region of the RR (covered in the J- and nbL-band data). This is corroborated by the HK spectropolarimetry (Fig. 2), which is essentially sampling the bright unresolved central peak, and which also shows the polarization to be around 1 per cent or lower between 1.4 and 2.5 μm. **If the central bicone were polarized then, because of the axisymmetry of the structure, we would expect to observe a net polarization signal in the integrated beam, even though that structure is unresolved in our observations. Examples of this effect, using a simple dust scattering model, are given in Fig. 6 of Gledhill (2005).** Also, the polarized light in the nebula, seen in Fig. 1, must result from scattering of light originating from the lobes of the central bicone, because for lines of sight outside the bicone, the post-AGB star itself remains obscured to dust particles in the surrounding envelope, even in the infrared. If this light was strongly polarized, and then re-scattered in the extended nebula, we would expect significant deviations from a centrosymmetric polarization pattern. This is not observed, which again is consistent with the light emanating from the centre having a polarization less than 1 per cent.

The low polarization of the central bicone in the near-infrared suggests that it is not seen by scattered light. The problem then arises that, if the bicone walls of the RR contain large 2 mm-radius dust spheres as modelled by M02, we would expect them to scatter and appear highly polarized in the J-band. Fig. 4 shows a polarization curve for a 2 mm-radius sphere of amorphous carbon. At such large size parameters ($x = 2\pi a/\lambda > 10^4$), geometric optics applies, and the curve in Fig. 4 is valid for optical and near-IR wavelengths. A peak polarization of 90 per cent is reached. Given that we have not measured polarization greater than 1 per cent at the centre of the RR between 1.2 and 3.4 μm, it seems unlikely that the bicone results from scattering from very large spherical particles.

Of course, spherical particles are a simplistic assumption ususally introduced for computational convenience, and any large grains in the RR are likely to have a more complicated structure. Does scattering from large irregular particles result in low polarization? Rough spheres and more irregular agglomerate particles have been considered as a model for interplanetary dust particles (IDPs) and for cometary dust. Weiss-Wrana (1983) conclude that the optical properties of the zodiacal light, including a peak polarization of 35 per cent at scattering angle 85°, can be produced by very rough and dark IDPs with sizes between 10 and 100 μm. The implication here is that large ($x > 400$) irregular particles can generate large polarization. Also, Kimura, Kolokolova & Mann (2003) find that fractal clusters of submicron 'monomers' have similar polarizing characteristics to cometary dust, resulting in optical polarizations of tens of per cent. Although these clusters are sub-micron in size and therefore much smaller than the suspected particle sizes in the RR, extension of the work to larger cluster sizes (Kimura & Mann 2004) gives similar results. Hadamcik et al. (2007) experiment with laboratory samples of agglomerations made up of larger micron-sized grains, which are either levitated or deposited onto a flat surface. These particles can also produce polarizations up to 20 per cent, as long as they have low albedo.

Although it is not clear that these materials can be considered as analogues for large grains in the RR, it does seem that large irregular particles can produce significant polarization by scattering. An alternative possibility is that the dominant component of infrared emission from the central bicone is not scattered but produced *in situ*, as thermal emission from hot dust and/or from particle emission, and hence instrinsically unpolarized. The near-infrared emission from the bicones shows a featureless continuum, rising from around ~ 1 to ~ 3.5 μm (see Fig. 3 of M02 and Fig. 2 of this paper) whereas the stellar spectrum falls steeply over the same wavelength range. A large particle dust model would not have such a strongly wavelength dependent albedo and so the near-infrared excess is more readily explained as emission by hot dust, than by scattering, and would therefore be unpolarized. The peak temperature of the large grains at the inner 14 au radius of the dust envelope in the M02 model is $\sim$ 1000 K, corresponding to the sublimation radius within which grains are destroyed. However, this dust would be located within and totally obscured by the dark lane. The peaks of the bicones are roughly $\pm$100 mas (70 au) above and below the dark lane in the images of Tuthill et al. (2002) where, assuming the same emissivity, the equilibrium dust temperature would be $\sim$ 500 K. These warm grains (both large and small) can be expected to contribute to the observed rising infrared continuum. A further source of near-infrared emission is likely to be from nanoparticles which are blown out from the central region through the bicone openings and which will retain very high emission temperatures as a result of non-equilibrium temperature

fluctuations as they absorb direct radiation from the central source. Dust emission, both equilibrium and stochastic, is radiated isotropically whereas scattered light is forward-peaked and hence beamed out along the bicone axis. As a consequence, the ratio of nanoparticle emission to scattering by larger grains increases sharply as a function of angular offset along the bicone axis. A determination of the contributions of scattered and intrinsic emission to the appearance of the central region of the RR could be obtained using high spatial resolution imaging polarimetry.

5 CONCLUSIONS

We present J and H broad-band, and 3.4 μm narrow-band imaging polarimetry of the Red Rectangle which reveals a near-infrared reflection nebula around the stars. The scattered light is concentrated in an equatorial region at J and H, and elongated perpendicular to the optical bicones seen in the light of ERE. We identify the polarized light with the dust component of the molecular envelope recently detected in CO, with which it is aligned, and whose inner region has been modelled as a rotating disc. This flattened dust envelope also appears to be the location for the recently discovered Blue Luminescence.

The degrees of infrared polarization are low, being 2-4 per cent at J and lower at longer wavelengths. At J and H this is consistent with dilution by an overlying unpolarised PSF, originating from the bright central bicone, which remains unresolved in our observations. In the nbL (3.4 μm) filter, unpolarized emission from the nebula dominates the scattering, which is restricted to the central region. We find that the amorphous carbon dust model used by Men'shchikov et al. (2002) to fit the SED of the RR is consistent with the observed polarization.

However, the same model invokes very large particles in the central dust shell, and it is difficult to reconcile scattering from these particles with our observations. In particular, scattering from large spheres should produce very high polarization at optical to near-infrared wavelengths, for which we find no evidence. It is likely that the rising near-infrared continuum, which dominates the spectrum in the central region of the RR, results from unpolarized emission by hot dust grains in equilibrium with the central source as well as emission from nanoparticles that are momentarily heated to high temperatures. Further high spatial resolution polarimetric observations of the central bicone would be helpful in determining the relative contributions of scattering and emission in the RR.

ACKNOWLEDGMENTS

We thank the staff of the UK Infrared Telescope for their assistance with the observations. The UK Infrared Telescope is operated by the Joint Astronomy Centre on behalf of the Science and Technology Facilities Council. ANW and UPV acknowledge support from the US National Science Foundation through grant AST0606756 to the University of Toledo.

REFERENCES

Aitken D.K. & Hough J.H., 2001, PASP, 113, 1300
Allamandola L.J., Tielens A.G.G.M., Barker J.R., 1985, ApJ, 290, 25
Bujarrabal V., Neri R., Alcolea J., Kahane C., 2003, A&A, 409, 573
Bujarrabal V., Castro-Carrizo A., Alcolea J., Neri R., 2005, A&A, 441, 1031
Cohen M.,et al., 1975, ApJ, 196, 179
Cohen M., Van Winckel H., Bond H.E., Gull T.R., 2004, AJ, 127, 2362
Gledhill T.M., Chrysostomou A., Hough J.H., Yates J.A., 2001, MNRAS, 322, 321
Gledhill T.M., 2005, MNRAS, 356, 883
Hadamcik E., Renard J.-B, Lasue J., Levasseur-Regourd A.C., Blum J., Schraepler R., 2007, JQSRT, 106, 74
Hora J.L., Deutsch L.K., Hoffmann W.F., Fazio G.G., 1996, AJ, 112, 2064
Jones T.J., Dyck H.M., 1978, ApJ, 220, 159
Jura M., Turner J., Balm S.P., 1997, ApJ, 474, 741
Kimura H., Kolokolova L., Mann I., 2003, A&A, 407, L5
Kimura H., Mann I., 2004, JQSRT, 89, 155
Lucas P.W., Roche P.F., 1998, MNRAS, 299, 699
Mékarnia D., Rouan D., Tessier E., Dougados C., Lefèvre J., 1998, A&A, 336, 648
Men'shchikov A.B., Balega Y.Y., Osterbart R., Weigelt G., 1998, New Astronomy, 3, 601
Men'shchikov A.B., Schertl D., Tuthill P.G., Weigelt G., Yungelson L.R., 2002, A&A, 393, 867
Miyata T., Kataza H., Okamoto Y.K., Onaka T., Sako S., Honda M., Yamashita T., Murakawa K., 2004, A&A, 415, 179
Perkins H.G., Scarrott S.M., Murdin P., Bingham R.G., 1981, MNRAS, 196, 635
Preibisch Th., Ossenkopf V., Yorke H.W., Henning Th., 1993, A&A, 279, 577
Ramsay Howat S.K., et al., 2004, Proceedings of SPIE, 5492, 1160
Reese M.D., Sitko M.L., 1996, ApJ, 467, L105
Russell R.W., Soifer B.T., Willner S.P., 1978, ApJ, 220, 568
Schmidt G.D., Cohen M., Margon B., 1980, ApJ, 239, L133
Sellgren K., Werner M.W., Dinerstein H.L., 1992, ApJ, 400, 238
Sellgren K., Werner M.W., Allamandola L.J., 1996, ApJS, 102, 369
Song I-O., Kerr T.H., McCombie J., Sarre P.J., 2003, MNRAS, 346, L1
Thronson H.A., 1982, AJ, 87, 1207
Tuthill P.G., Men'shchikov A.B., Schertl D., Monnier J.D., Danchi W.C., Weigelt G., 2002, A&A, 389, 889
Van Winckel H., Waelkens C., Waters L.B.F.M., 1995, A&A 293, L25
Vijh U.P., Witt A.N., Gordon K.D., 2004, ApJ, 606, L65
Vijh U.P., Witt A.N., York D.G., Dwarkadas V.V., Woodgate B.E., Palunas P., 2006, ApJ, 653, 1336
Waters L.B.F.M. et al., 1998, Nature, 391, 868
Weiss-Wrana K., 1983, A&A, 126, 240
Whittet D.C.B., Martin P.G., Hough J.H., Rouse M.F., Bailey J.A., Axon D.J., 1992, ApJ, 386, 562

Witt A.N., York D.G., Hobbs L.M., Vijh U.P., Aufdenberg J.,
Thorburn J.A., 2008, ApJ in preparation